RECEIVED BEST PAPER AWARD

Reprinted From
HTD – Vol. 106, Heat Transfer Phenomena in Radiation, Combustion, and Fires
Editor: R. K. Shah
Book No. H00498 – 1989

The American Society of Mechanical Engineers

LIQUID JET IMPINGEMENT HEAT TRANSFER ON A UNIFORM FLUX SURFACE

X. Liu and J. H. Lienhard V
Department of Mechanical Engineering
Massachusetts Institute of Technology
Cambridge, Massachusetts

ABSTRACT

Convective heat transfer to an impinging liquid jet is investigated. A circular jet of subcooled liquid impinges on a heating surface maintained at a uniform heat flux. An integral method is used to obtain analytical predictions of the temperature distribution in the liquid film and the local Nusselt number. As a result of the radial development of the viscous and thermal boundary layers and of the film thickness, several characteristic heat transfer regions appear. The variation of Nusselt number is different in each region.

Experiments were performed to test the predictions of the theory. Subcooled water jets leaving a circular orifice cooled an electrically heated sheet under atmospheric conditions. The radial temperature distribution was measured and the Nusselt number was computed as a function of the jet Reynolds number. Agreement between the predictions and the experiments is generally good. Several factors are identified which may cause differing behavior outside a laboratory environment.

NOMENCLATURE

Roman Letters

A function defined in equation (10).

C_2, C_3, C_4 constants of integration.

c_p liquid specific heat capacity.

d jet diameter.

g_m local mass transfer coefficient from liquid surface to environment.

$h(r)$ local thickness of liquid sheet.

$\hat{h}$ local heat transfer coefficient from liquid surface to environment.

h_{fg} latent heat of vaporization.

h_{r_1} liquid sheet thickness at $r = r_1$.

k thermal conductivity of the liquid.

m_w, m_∞ water vapor mass fractions at liquid surface, in environment.

Nu_r Nusselt number, $qr/k(T_w - T_f)$.

Nu_x Nusselt number, $qx/k(T_w - T_f)$.

p, s parameters defined in equation (19).

q wall heat flux.

r radius measured from point of jet impact.

r_o radius at which δ reaches the surface of the liquid sheet.

r_1 radius at which δ_t reaches the surface of the liquid sheet.

r_2 radius at which T_w reaches the liquid saturation temperature.

Re_d Reynolds number of the jet, $u_f d/\nu$.

Sc Schmidt number for water vapor in air.

$T(r, y)$ liquid temperature distribution.

T_f jet temperature at impingement.

$T_{f4}(r)$ jet surface temperature distribution in region 4.

T_{sat} liquid saturation temperature.

$T_w(r)$ wall temperature distribution.

$u(r, y)$ radial velocity distribution in liquid film.

u_f velocity of impinging jet.

u_{max} local maximum film velocity (liquid surface velocity), equal to u_f in region 2.

y distance normal to the wall.

Greek Letters

δ viscous boundary layer thickness.

δ_t thermal boundary layer thickness.

η normalized velocity just outside the boundary layer, u/u_f.

θ jet impingement angle.

μ dynamic viscosity.

ν kinematic viscosity.

ρ density.

INTRODUCTION

Jet impingement cooling has broad application, such as controlled cool-

ing of metals or non-metals in manufacturing processes, as a result of its easy implementation and high efficiency. Many investigations have dealt with convective heat transfer by submerged jet impingement (gas jets in gases or liquid jets in liquids), but studies of free liquid jets (travelling through gases) are much less common, particularly those presenting theoretical analyses of the heat transfer by liquid jets. The reason may be the complexity of the local phenomena.

When a liquid jet strikes a flat surface, it spreads radially in a thin film. This film is responsible for convective heat removal form the surface. Following Watson (1964), we subdivide the jet impingement flow into four regions:

1. *The stagnation zone.*
2. *The boundary layer region.* In this region, the viscous boundary layer thickness is less than the liquid sheet thickness, so that the liquid on the surface is unaffected by wall friction.
3. *The fully viscous sheet.* In this region, the boundary layer thickness is the same as the sheet thickness. The viscous influence extends through the entire liquid film, from the wall to the free surface.
4. *The hydraulic jump.* An abrupt increase of liquid sheet thickness occurs, and in this region the liquid velocity is much lower than in the upstream region.

Watson analyzed the hydraulic jump by an inviscid theory and regions 2 and 3 by a similarity solution of the boundary layer equations. Sharan (1984) applied the momentum integral method to analyze regions 2 and 3 and obtained results in good agreement with those of Watson.

McMurray *et al.* (1966) studied convective heat transfer to impinging *plane* jets from uniform heat flux walls. They observed the heat transfer to be subdivided into an impingement zone and a zone of uniform parallel flow. To fit their data, they based heat transfer correlations on the stagnation flow in the impingement zone and on the flat plate boundary layer in the uniform parallel flow zone. They obtained results in the form

$$\mathrm{Nu}_x = f(\theta, \eta, \mathrm{Re}_x, \mathrm{Pr}) \qquad (1)$$

where θ is the angle of impingement and η is jet velocity normalized with that just outside the boundary layer, u/u_f.

Chaudhury (1964) solved the axisymmetric energy equation for a constant wall temperature condition in the fully viscous region, where a similarity solution of the momentum equation is available. The solution was expressed as a series expansion.

Metzger *et al.* (1974) experimentally studied the effects of Prandtl number on heat transfer by liquid jets. They used a uniform surface temperature boundary condition at the test surface. They presented only surface average values of the Stanton number, determined from measurement of the total heat flux, the test surface temperature, and the jet adiabatic wall temperature. No local measurements or analytical results were given. Their correlations are based on data for oil and water; for water, their correlation represents 95% of the data for disk radii of up to 6.6 jet diameters to within ±25%. The possible effect of evaporation resulting from apparently high liquid surface temperatures was not documented.

Carper *et al.* (1978,1986) studied the heat transfer from a rotating disk struck by a liquid jet. The papers show that disk rotation enhances the heat transfer

In the present paper, an integral method is used to predict the Nusselt number for constant heat flux and to examine the distance required to reach liquid saturation temperatures (relevant to the boiling jet problem). In a corroborating experiment, the wall temperature distribution was measured for positions up to 43 jet diameters from the point of impact and the local values of the Nusselt number were calculated. The analytical results are compared to the experimental data. Although the predictions of the theory are not simple, we hope that simplified correlations for convective heat transfer by jet impingement can be developed on the basis of these more complicated results.

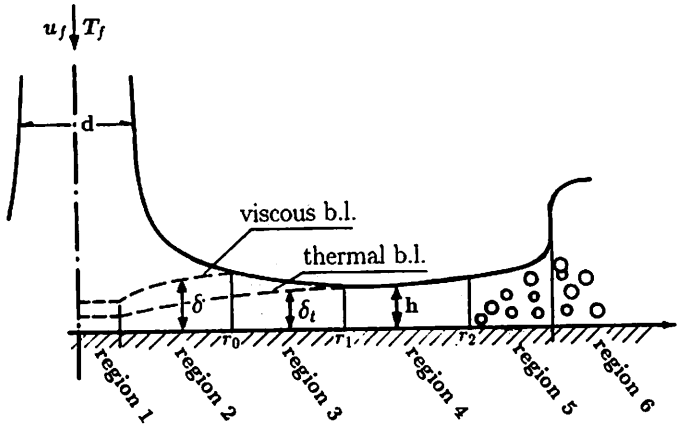

Figure 1: Region map for the downward-flowing jet.

Heat Transfer Regions

The heat transfer regions are more complicated than those of the flow field because more parameters are involved. We shall assume that the Prandtl number is greater than unity, Pr > 1, as is the case for most liquids. The heat transfer regions can then be subdivided as follows (*see* Figure 1).

1. *The stagnation zone.*
2. $\delta < h$ *region*: Within this region, the velocity outside the viscous boundary layer is undisturbed and approximately equal to the jet velocity, u_f.
3. $\delta = h$ *and* $\delta_t < h$ *region*: Within this region, the temperature outside the thermal boundary layer is not affected by the heat transfer, but the thermal boundary layer is affected by the viscous retardation of the momentum boundary layer.
4. $\delta = h, \delta_t = h$, *and* $T_w < T_{sat}$ *region*: In this region, the thermal boundary layer has reached the surface of the liquid sheet, and the temperature of the liquid surface increases with radius. Our analysis below shows that this region cannot exist for Pr > 4.859.
5. *The boiling region:* This region may include regions of nucleate boiling, burnout, and dry surface if the heat flux is high enough. Since boiling might occur at any wall temperature beyond T_{sat}, depending on heater finish and other factors, we will refer to the entire region for which $T_w > T_{sat}$ as the boiling region. We avoid all detailed consideration of nucleation incipience in the present work.
6. *The hydraulic jump:* In this region the heat transfer deteriorates dramatically. If the jet is directed upward (Figure 2), the hydraulic jump is very different than for the downward-directed jet. In that case, the jump is associated with a Rayleigh-Taylor instability. This instability will be discussed in a separate paper.

In the present paper, we do not treat region 5 or region 6. It must be noted that the all of the above regions may not exist at the same time, and that the last two may occur in a different sequence. For example, boiling incipience may take place in any region, and it can change the region map. The hydraulic jump may even occur in region 2 for low heat flux.

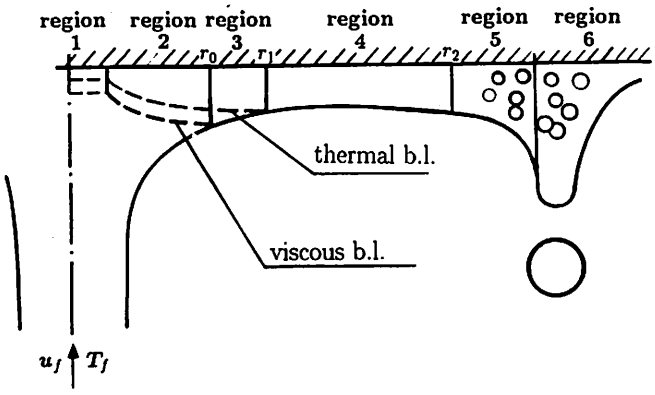

Figure 2: Region map for the upward-flowing jet.

We note in passing that for Pr < 1, region 2 and region 3 will instead be:

2. $\delta < h$ *region:* Since Pr < 1, the viscous boundary layer is thinner than the thermal boundary layer.

3. $\delta_t = h$ *and* $\delta < h$ *region:* In this region, the thermal boundary layer has reached the surface while the viscous boundary layer has not.

For the constant wall temperature problem, the region map would be simpler since we know in advance whether or not boiling occurs. In the present paper, we consider the regions 2, 3, and 4 without boiling for a uniform wall heat flux with Pr > 1.

ANALYSIS

Region 2

Sharan (1984) shows that treating the flow as purely radial is a very good approximation. We assume that in the regions beyond region 1, a purely radial flow occurs. In these regions, the integral energy equation is given by

$$\frac{d}{dr}\int_0^{\delta_t} ru(T-T_f)\,dy = \frac{q}{\rho c_p}r \tag{2}$$

where T is the liquid temperature profile, T_f is the subcooled incoming jet temperature, q is the uniform wall heat flux, u is the radial liquid velocity profile, and other terms are defined in the nomenclature. We approximate the profiles in equation (2) as:

$$T - T_w = (T_f - T_w)\left[\frac{3}{2}\frac{y}{\delta_t} - \frac{1}{2}\left(\frac{y}{\delta_t}\right)^3\right] \tag{3}$$

$$u = u_{max}\left[\frac{3}{2}\frac{y}{\delta} - \frac{1}{2}\left(\frac{y}{\delta}\right)^3\right] \tag{4}$$

for T_w the wall temperature and $u_{max} = u_f$ the constant liquid surface speed in region 2. For Pr > 1, we neglect $3\delta^3/280\delta_t{}^3$ relative to $3\delta/20\delta_t$ and integrate to obtain

$$\frac{27}{80}\mathrm{Re}_d\mathrm{Pr}\frac{1}{\mathrm{Nu}_r^3}\left(\frac{r}{d}\right)^2\frac{r^2}{\delta d} = \frac{1}{2}\left(\frac{r}{d}\right)^2 + C_2 \tag{5}$$

where $\mathrm{Nu}_r = qr/k(T_w - T_f)$ and $\mathrm{Re}_d = u_f d/\nu$.

For $d/2 \ll r$, Sharan shows that the initial boundary layer thickness can be neglected. We have the same situation for the thermal boundary layer and may use Sharan's expression for δ

$$\delta = 2.679\left(\frac{rd}{\mathrm{Re}_d}\right)^{1/2} \tag{6}$$

Thus, we find

$$\mathrm{Nu}_r = 0.632\,\mathrm{Re}_d^{1/2}\mathrm{Pr}^{1/3}\left(\frac{r}{d}\right)^{1/2} \tag{7}$$

At $r = r_o$, the viscous boundary layer reaches the surface of the liquid sheet, which is the border of region 2. Sharan gives

$$r_o = 0.1773\,\mathrm{Re}_d^{1/3}d \tag{8}$$

Region 3

The significant difference between this region and region 2 is that in this region the velocity at the liquid surface, u_{max}, is not constant. Watson (1964) and Sharan (1984) show

$$u_{max} = \frac{A}{hr} = \frac{1}{5}\frac{u_f d^2}{hr} \tag{9}$$

where

$$A = \frac{u_f d^2}{5} \tag{10}$$

and

$$h = 0.1713\left(\frac{d^2}{r}\right) + \frac{5.147}{\mathrm{Re}_d}\left(\frac{r^2}{d}\right) \tag{11}$$

In this region, the energy equation is again equation (2), but u_{max} is now a function of r and h and $\delta = h$. Integration with equations (3), (4), and (9), neglecting higher order terms as before, gives

$$\frac{3}{100}\mathrm{Re}_d\mathrm{Pr}\frac{1}{\mathrm{Nu}_r}\left(\frac{\delta_t}{h}\right)^2\frac{r}{d} = \frac{1}{2}\left(\frac{r}{d}\right)^2 + C_3 \tag{12}$$

With

$$\mathrm{Nu}_r = 3r/2\delta_t \tag{13}$$

from equation (3), substitution of equation (11) into equation (12) and subsequent rearrangement then yields

$$\mathrm{Nu}_r = \frac{0.407\,\mathrm{Re}_d^{1/3}\mathrm{Pr}^{1/3}(r/d)^{1/3}}{\left[0.1713\left(\frac{d}{r}\right)^2 + \frac{5.147}{\mathrm{Re}_d}\frac{r}{d}\right]^{2/3}\left[\frac{1}{2}\left(\frac{r}{d}\right)^2 + C_3\right]^{1/3}} \tag{14}$$

From equation (8), at $r = r_o$

$$\mathrm{Nu}_r = 0.632\,\mathrm{Re}_d^{1/2}\,\mathrm{Pr}^{1/3}\left(\frac{r_o}{d}\right)^{1/2} \tag{15}$$

Solving equations (14 - 15) for C_3 produces

$$C_3 = \frac{0.267(d/r_o)^{1/2}}{\left[0.1713\left(\frac{d}{r_o}\right)^2 + \frac{5.147}{\mathrm{Re}_d}\frac{r_o}{d}\right]^2\mathrm{Re}_d^{1/2}} - \frac{1}{2}\left(\frac{d}{r_o}\right)^2 \tag{16}$$

At $r = r_1$, the border of region 3, we have $\delta_t = h$. To locate r_1, we use equations (13) and (12) to find

$$\frac{2}{100}\mathrm{Re}_d\mathrm{Pr}\left(\frac{h}{d}\right) = \frac{1}{2}\left(\frac{r}{d}\right)^2 + C_3 \tag{17}$$

Then, using equation (11) and rearranging, we get

$$\left(\frac{r_1}{d}\right)^3 + p\left(\frac{r_1}{d}\right) + s = 0 \tag{18}$$

where we define

$$p = \frac{-2C_3}{(0.2058\,\mathrm{Pr} - 1)} \qquad s = \frac{0.00686\,\mathrm{Re}_d\mathrm{Pr}}{(0.2058\,\mathrm{Pr} - 1)} \tag{19}$$

Since C_3 is usually less than zero, equation (18) has real, positive roots when

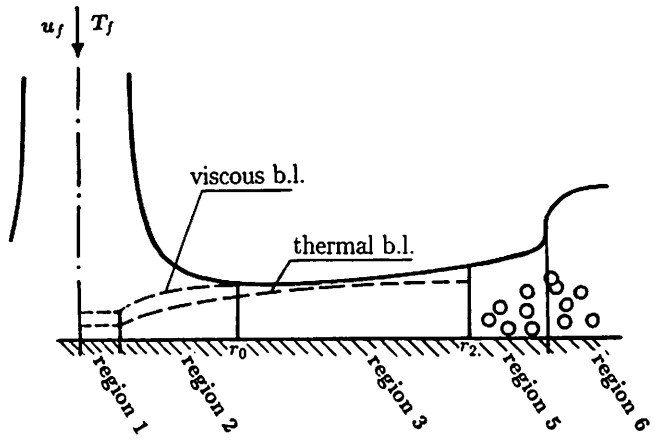

Figure 3: Region map for Pr > 4.859.

$$s < 0 \tag{20}$$

This condition is satisfied only for

$$\mathrm{Pr} < 4.859 \tag{21}$$

This is a very interesting result. It means that for Pr > 4.859 the thermal boundary layer can never reach the surface of the liquid sheet before subcooled boiling occurs: the increase of h owing to viscous retardation is more rapid than the growth of the thermal boundary layer.[1] In this case, region 4 cannot exist. The situation is shown schematically in Figure 3.

For Pr < 4.859, equation (18) yields

$$\frac{r_1}{d} = \left\{-\frac{s}{2} + \left[\left(\frac{s}{2}\right)^2 + \left(\frac{p}{3}\right)^3\right]^{1/2}\right\}^{1/3} + \left\{-\frac{s}{2} + \left[\left(\frac{s}{2}\right)^2 - \left(\frac{p}{3}\right)^3\right]^{1/2}\right\}^{1/3} \tag{22}$$

With this and equation (11), we can calculate the liquid sheet thickness, h_{r1}, at $r = r_1$. The wall temperature can be determined from the expression

$$T_w = T_f + \frac{q\,r}{k\,\mathrm{Nu}_r} \tag{23}$$

Since boiling might occur for any wall temperature which exceeds the saturation temperature, depending on heater surface finish and other factors, we exclude any case for which $T_w > T_{sat}$ from subsequent considerations.

Region 4

For Pr < 4.859, after the thermal boundary layer reaches the surface, the surface temperature increases with radius. If we neglect the heat transfer from the liquid surface, the energy equation may be written

$$\frac{d}{dr}\int_0^h ruT\,dy = \frac{q}{\rho c_p}\,r \tag{24}$$

We assume the temperature profile to be

$$T - T_w = (T_{f4} - T_w)\left[\frac{3}{2}\frac{y}{h} - \frac{1}{2}\left(\frac{y}{h}\right)^3\right] \tag{25}$$

where the surface temperature in region 4, T_{f4}, is a function of r. Substituting equations (4), (9), and this temperature distribution into

[1]The precise value of Pr will be affected by the various minor approximations inherent in the integral solutions of the transport equations. Historically, integral solutions have shown good agreement with exact solutions in spite of the approximations involved.

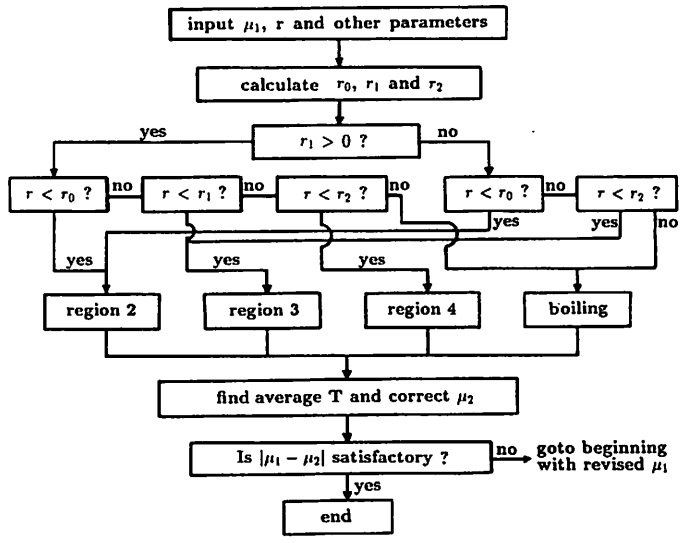

Figure 4: Calculation procedure for integral predictions.

equation (24), we obtain

$$A\left(\frac{5}{8}T_{f4} + \frac{13\,qh}{140\,k}\right) = \frac{q}{\rho c_p}\frac{r^2}{2} + C_4 \tag{26}$$

The constant may be found by evaluating this expression at $r = r_1$, where $T_{f4} = T_f$ and $h = h_{r1}$:

$$C_4 = A\left(\frac{5}{8}T_f + \frac{13\,q\,h_{r1}}{140\,k}\right) - \frac{q}{\rho c_p}\frac{r_1^2}{2} \tag{27}$$

Since $T_{f4} = T_w - 2qh/3k$,

$$\mathrm{Nu}_r = \frac{0.25\,(r/d)}{\frac{1}{\mathrm{PrRe}_d}\left(1 - \frac{r_1^2}{r^2}\right)\left(\frac{r}{d}\right)^2 + 0.130\frac{h}{d} + 0.0371\frac{h_{r1}}{d}} \tag{28}$$

and

$$T_w = T_f + \frac{q}{k}\left[0.518\,h + \frac{4\alpha(r^2 - r_1^2)}{u_f\,d^2} + 0.149\,h_{r1}\right] \tag{29}$$

From equation (29) we can find r_2, the point at which T_w exceeds the saturation temperature, and beyond which subcooled boiling might occur. We exclude consideration of the region $r > r_2$ from this paper.

Calculations

To use these results in calculating Nu_r and $T_w(r)$, a numerical iteration is most expedient. In particular, the viscosity varies strongly with temperature for most liquids, and properties must be evaluated at the local average temperature across the film. The some of the different expressions for each region are also quite complex. The flowchart in Figure 4 shows the general procedure for using the analytical results of this section to determine the distribution of Nusselt number and wall temperature. This procedure was used in obtaining the calculated results presented in Section 4 below.

EXPERIMENTS

To verify the predictions of the preceding sections, experiments were performed with water jets under atmospheric conditions. The radial wall temperature distributions beneath a jet striking a uniformly electrically heated surface were measured, and the data were used to calculate the local values of the Nusselt number. In this section, the

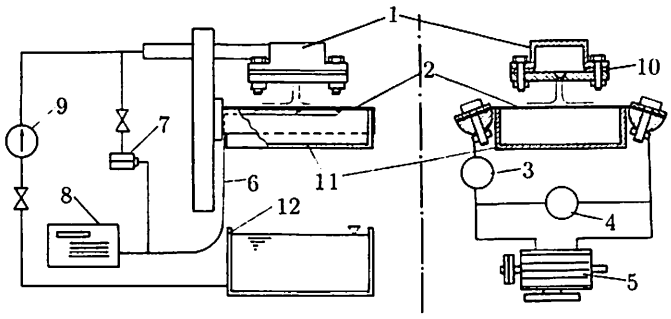

Figure 5: Experimental Apparatus: 1. orifice and plenum; 2. test surface; 3. ammeter; 4. voltmeter; 5. generator; 6. thermocouples; 7. pressure transducer; 8. digital voltmeter; 9. pump; 10. gasket; 11. plastic box; 12. water tank.

experimental procedure is described. The data and the theory are compared in the next section.

Experimental Apparatus

The experimental apparatus is shown schematically in Figure 5. An orifice plate faces vertically downward toward an electrically heated plate. The plate temperature was measured for water jets of differing diameter and speed hitting the plate when heated at different fluxes.

The electric heater is made of stainless steel sheet 0.10 mm thick. The variation in thickness of the steel plate is about ±3%. The working dimensions of the sheet are 7.8 cm by 15.2 cm. This sheet is clamped at either end onto the flat surfaces of two 5.1 cm diameter hemispherical copper rods which span the entire 15.2 cm width of the heater sheet. The rods are connected to a low voltage, high current generator, thus causing Joule heating of the steel sheet uniform to ±6%. Conductive heat loss to the rods was estimated to be negligible as a result of the thinness of the sheet and the low temperature differences involved.

The sheet temperature distribution was measured by twelve evenly-spaced thermocouples along a radial line parallel to the copper rods and passing through the point of jet impact. The thermocouples were each attached to the underside of the heater sheet with glue and were electrically separated from it by a thin wafer of mica. The thickness of the mica sheets is less than 0.015 mm and the thermal conductivity is not less than 5 W/(mK); the thermal resistance of the mica is negligible compared to that of the natural convection and the thermalcouple temperatures were within ±0.01°C of the plate surface temperatures. The back of the heater and the thermocouples were covered with an air filled plastic box which kept them dry and isolated them from room air currents. Free convection heat losses through the back of the heater were estimated to be negligible ($\approx 10 W/m^2$) because the heater temperatures were quite low.

Subcooled water, near room temperature, was supplied to the orifice through a high pressure pump. The rise in water supply temperature was slow compared to the time required for measurement of the radial temperature profile, and the inlet water temperature was thus effectively constant for each profile. The plenum behind the orifice is supplied by a 2.54 cm ID pipe. The plenum was 5.08 cm in diameter and 3.18 cm deep. The orifice plate covered this plenum; the orifice was a small hole with countersunk entry drilled in the center of the plate. The gauge pressure upstream of the plenum was recorded with a pressure transducer, and the jet velocities were computed from it using the standard jet relations. The jet struck the sheet halfway between the two rods and 2.8 cm from one edge. The precise effects of this azimuthal asymmetry on the flow field may warrant further study.

Pump pressure fluctuations were damped using an accumulator upstream of the orifice plenum. However, turbulence present in the inlet pipe and plenum still led to some minor fluctuations in the jet surface. These fluctuations gave rise to intermittent splattering downstream in the liquid sheet on the heater plate. The total volume of liquid leaving the surface as droplets was small compared to that remaining in the film. The average effects of this splattering are discussed further in the following section. Errico and Middleman (1986) have discussed the mechanisms of splattering in detail.

Table 1: Measured Nusselt number for water under atmospheric conditions.

$q = 12.4 \times 10^4$, $d = 2.58$ mm				
	Re_d			
r/d	3.54×10^4	4.50×10^4	5.27×10^4	6.24×10^4
3.38	436	440	479	544
7.75	599	651	713	787
11.6	590	748	831	897
15.5	544	665	767	880
19.4	499	584	692	763
23.3	462	528	599	660
27.1	385	436	569	504
31.0	313	413	507	549
34.9	289	389	449	492
38.8	250	261	398	399
42.6	211	256	361	282

$q = 7.73 \times 10^3$, $d = 3.05$ mm		
	Re_d	
r/d	4.03×10^4	5.89×10^4
3.28	424	484
6.56	549	669
9.84	667	781
13.1	434	853
16.4	417	718
19.7	394	640
23.0	403	731
26.2	401	578
29.5	336	536
32.8	307	432
36.1	175	308

$q = 17.2 \times 10^4$, $d = 2.58$ mm	
	Re_d
r/d	41.5×10^4
3.88	489
7.75	686
11.6	752
15.5	686
19.4	604
23.3	528
27.1	491
31.0	437
34.9	394
38.8	314
42.6	233

Experimental data were obtained for orifice diameters from 2.58 to 3.05 mm, heat fluxes from 7.73×10^3 to 17.2×10^4 W/m^2, and jet velocities in the range 12 to 24 m. The measured values of Nu_r and T_w are presented in Table 1 as a function of r/d for various q and Re_d. Experimental uncertainties in q and Re_d were estimated to be about 2%. The experimental uncertainty in Nu_r drops from about 13% at the smallest r/d to 1% at the largest r/d; it is associated primarily with the measurement of temperature difference, which is quite small near the point of jet impact.

RESULTS AND COMPARISONS

In this section, we consider the predictions of Section 2 in detail, and we discuss the results of the experiments performed to test the predictions. Experimental agreement with the predictions is generally good, although several effects present in real jets were discovered which can complicate the application of the theory to some non-laboratory systems.

The analytical predictions are compared to data for $q = 12.4 \times 10^4$ W/m^2 and $d = 2.58$ mm (our largest single data set) in Figure 6a. The radial variation of the Nusselt number, Nu_r, is shown for several values of the Reynolds number, Re_d, for r/d up to 43. The observed behavior may be related to the heat transfer regions defined in the analysis.

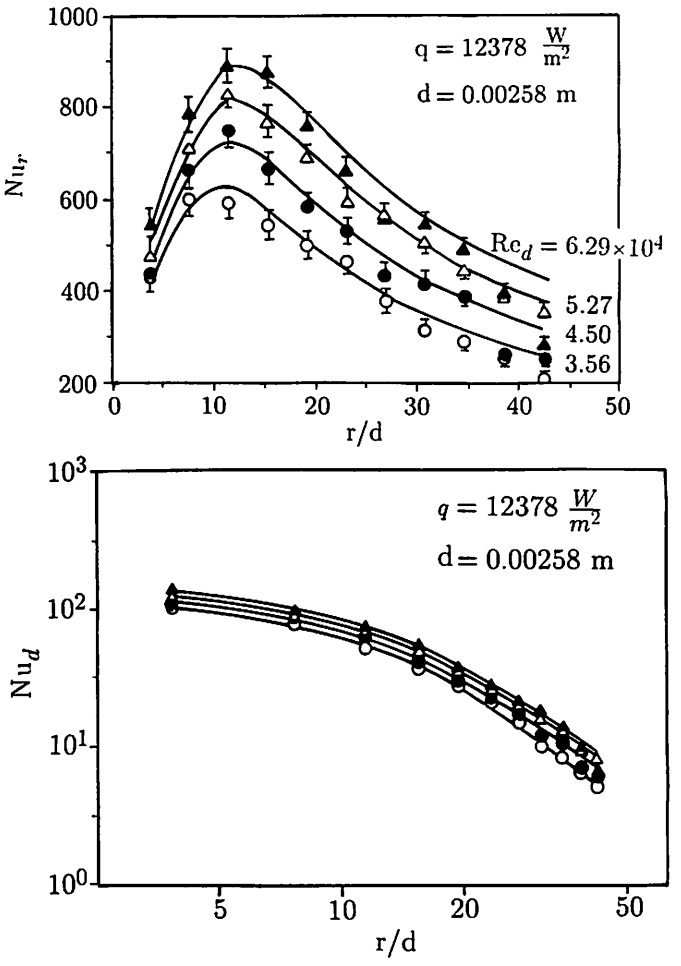

Figure 6: (a) Distribution of Nu_r: theory, —— ; data, ▲ $Re_d = 6.29\times10^4$, △ $Re_d = 5.27\times10^4$, • $Re_d = 4.50\times10^4$, ○ $Re_d = 3.56\times10^4$. (b) Distribution of Nu_d: theory, —— ; data, (symbols as before).

The Nusselt number increases over small values of r/d in regions 1 and 2 and the beginning of region 3; after reaching a maximum, it decreases for larger r/d in region 3. The boundaries of these regions change with Reynolds number, but we may cite typical values. Region 2 ends at $r = r_o$: for $Re_d = 3.54 \times 10^4$, $r_o/d = 5.81$; for $Re_d = 6.29 \times 10^4$, $r_o/d = 7.05$. For cases in which Pr< 4.859, the boundary of region 3, r_1, would be on the order of $78d$, beyond the range of this experiment, but the present flows all had Pr > 4.859. Since the inlet water temperature was 15°C, saturation temperatures would not be reached until $r_2 \approx 270d$, well beyond the experimental domain. The hydraulic jump, which was also beyond experimental range, would probably occur first in this situation.

If the Nusselt number is instead based on jet diameter, rather than the radius along the sheet, a monotonic decay is seen (Figure 6b). This shows directly the increase in surface temperature. The difference in magnitude of the Nusselt number among different values of the Reynolds number decreases at larger r/d, although this is not obvious on the logarithmic coordinates of Figure 6b.

For the data of Figure 6, the agreement between experiment and theory was about 3% for $r/d < 35$ and about 15% for $r/d > 35$. The agreement deteriorates at the largest radii, for reasons we now examine.

In our analysis, the evaporation from the liquid surface was neglected. This assumption should be carefully checked in any practical situation, since evaporative heat loss can become a significant fraction of the wall heat flux. Evaporation will tend to cool the liquid at the surface and reduce the rate of wall temperature increase (lowering Nu_r), even if only a very small amount of the liquid film is vaporized. The rate of evaporation increases rapidly with the surface temperature of the liquid; in dry air it will rise by a factor of 29 as the surface temperature increases from 5°C to 65°C. Some estimates are in order for the present data.

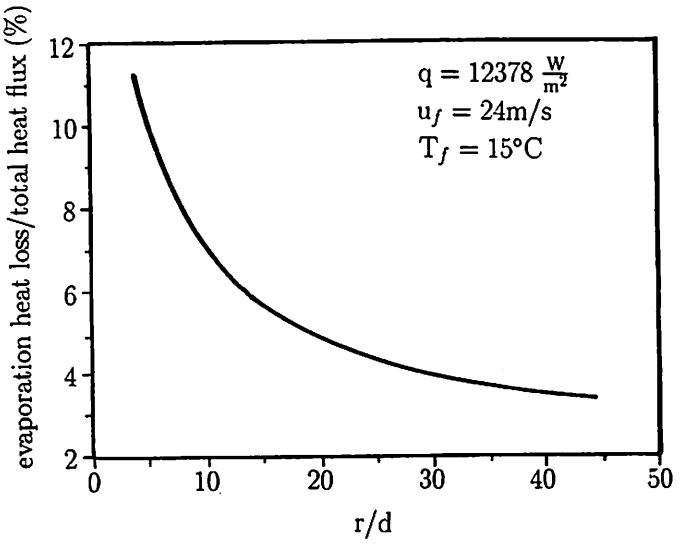

Figure 7: Estimated evaporative heat loss for the data of Figure 6 at $Re_d = 6.24 \times 10^4$.

The evaporative heat flux from the liquid surface can be calculated as

$$q_e = h_{fg}\, g_m (m_w - m_\infty) \tag{30}$$

where h_{fg} is the latent heat of vaporization, m_w is the mass fraction of water vapor at the liquid surface, m_∞ is the mass fraction of water in the environment, and the mass transfer coefficient, g_m, is calculated from the Lewis analogy

$$g_m = \frac{\hat{h}}{c_p}\left(\frac{\mathrm{Pr}}{\mathrm{Sc}}\right)^{2/3} \tag{31}$$

with $\hat{h}$ the estimated local heat transfer coefficient from the moving liquid to the air. For 15°C water, a wall heat flux of 12.4×10^4 W/m^2, and u_f = 24 m/s, the ratio of evaporative heat flux, q_e, to wall heat flux, q, is shown in Figure 7.

The heat flux by evaporation decreases rapidly with r/d. For $r/d > 20$, it is less than 5% of the wall heat flux, and it is never more than about 12% . The rapid decrease in q_e is due in part to the rapid slowing of the liquid surface velocity in region 3. While the evaporation is greatest in region 2, it has no effect on wall temperature until the surface and wall thermal boundary layers meet further downstream. The overall effect of evaporative cooling probably remains negligible in the present case because the overall reduction in liquid bulk temperature is only a few percent of the increase produced by wall heating. However, the same estimation procedure shows, for example, that for a surface temperature of 45°C, evaporation would become comparable to a wall flux of 12.4×10^4 W/m^2 and cannot be neglected.

A direct comparison between the analytical prediction and the data is given in Figure 8, where different symbols are used for small ($r/d < 35$) and large radius ($r/d > 35$) data for d = 2.58 mm and for the data at d = 3.08mm. The agreement is excellent for the d = 2.58 mm at $r/d < 35$, but shows larger errors further out. The d = 3.08mm shows larger error at all radii. Two major factors may be responsible for the deviation of the data from the prediction. One is surface evaporation, as discussed, and the other is splattering of liquid from the moving film. While evaporation tends to raise the Nusselt number, splatter decreases it by reducing the volume of liquid within

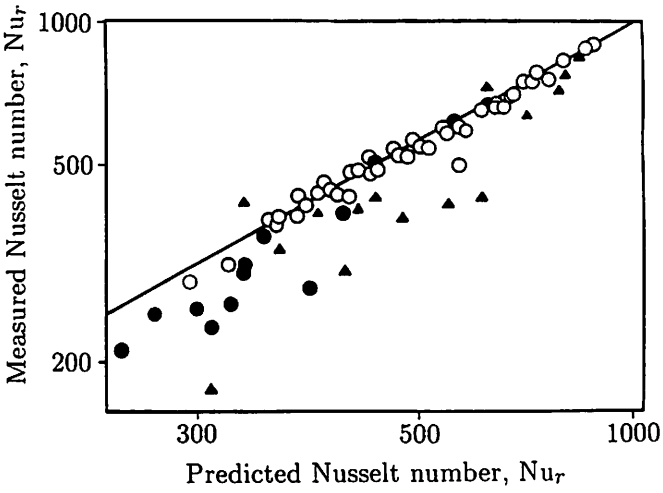

Figure 8: Comparison of predicted and measured Nusselt number: o, $d = 2.58$ mm, $r/d < 35$; •, $d = 2.58$ mm, $r/d > 38$; ▲, $d = 3.08$ mm.

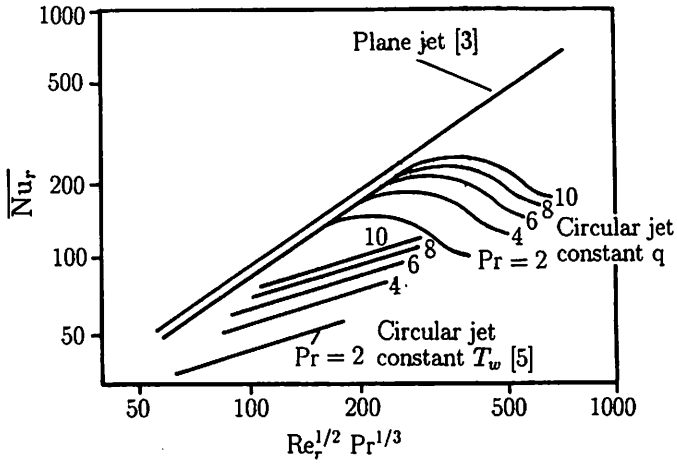

Figure 10: Comparison of predicted average Nusselt number for uniform flux to correlation for uniform wall temperature in circular jet impingement and to correlation for uniform flux plane jet impingement.

the film and producing an associated increase in the rate of rise of liquid bulk temperature. The effect of splatter accumulates in the film and is more serious downstream than upstream. In the present case, splattering is the dominant error.

The splattering of impinging liquid jets is driven by minor irregularities or unsteadiness in the incoming jet (in this case, by turbulence in the jet plenum) as discussed by Errico and Middleman (1986). The deviation of the measured and predicted Nusselt number in the region far from the center suggests that splatter may cause a decrease in the [time average] Nusselt number of more than 20% . No theoretical analysis predicts the effects of splatter; further experiments are needed in which splatter is both well controlled or eliminated.

The larger orifice ($d = 3.08$ mm) produced greater splatter and was run at lower heat flux. Both factors may contribute to the greater errors seen for that data.

Figure 9 shows a comparison of our prediction to the *plane* jet data of McMurray *et al.* (1966). The most significant difference is that, for the axisymmetric jet, Nu_r reaches a maximum and then decreases with radius, but that for the plane jet it does not. This is because

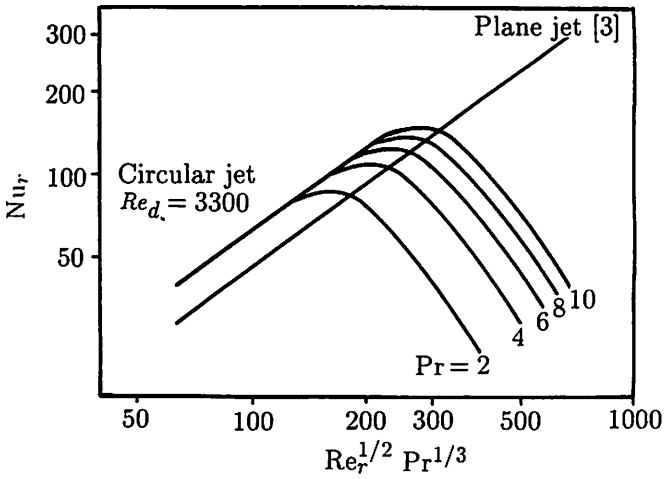

Figure 9: Comparison of predicted local Nusselt number for circular jets to local Nusselt number correlation for plane jets.

In Figures 9 and 10, Re_d is fixed at 3300. Thus, the variations of Re_r shown are variations of r at fixed jet speed u_j.

the liquid layer thickness produced by the plane jet of McMurray *et al.* was so large that the viscous boundary layer never reached the liquid surface. Thus, the differences are not surprising: McMurray's experiment remains in region 2 throughout. Before the boundary layer reaches the surface, the plane and axisymmetric jets show the same variation with Reynolds number, although for the axisymmetric jet the coefficient is 0.632 while for the plane jet it is 0.47, 25% lower.

Figure 10 compares the *average* Nusselt number for our uniform wall heat flux result to that for the uniform wall temperature axisymmetric jet experiments of Metzger *et al.* (1974). The average Nusselt number for a uniform wall heat flux is generally larger than that for a uniform wall temperature. Average Nusselt numbers for the uniform wall flux plane jet data of McMurray *et al.* are also shown. Although the local Nusselt number for the plane jet is smaller than for the axisymmetric jet in region 2 and part of region 3, the average Nusselt number for the plane jet is generally larger than that for the axisymmetric jet. In region 2, the average Nusselt number for the plane jet is twice as large as the local Nusselt number, but that for the axisymmetric jet is 4/3 the local one. This switch in size relates to the different areas involved in planar and axisymmetric averaging.

Observations in a separate apparatus show that, after the jet strikes the plate, the laminar flow formed in center region becomes wavy at some distance from center, finally becoming turbulent at a larger radius. The transition points for surface waves and for turbulence, and the heat transfer coefficient in turbulent region need further investigation. The divergence of our data and theory at large r/d may be related to such effects, although a turbulent region could not be observed directly in these experiments.

CONCLUSIONS

The heat transfer phenomena beneath an impinging circular jet can be divided into different regions by taking account of the development of the viscous and thermal boundary layers and the possible occurrence of nucleate boiling or a hydraulic jump. These regions may appear in different combinations, depending the jet Reynolds number, temperature levels, wall heat flux, and liquid physical properties. The radial variation of Nusselt number, Nu_r, is interpreted in terms of the development of the thermal boundary layer, and an integral analysis is

presented for each of the convective regions.

The analysis shows that if Pr > 4.859, the thermal boundary layer never reaches the surface of the liquid film because the growth of the thermal boundary layer is slower than the thickening of the liquid film caused by viscous retardation.

The prediction and present experimental results show that Nu_r reaches a maximum at some radius away from the point of impact and then decreases as the radius increases further. Both the magnitude and radial position of the maximum Nusselt number increase with Reynolds number. The wall temperature rises steadily away from the stagnation point.

Evaporative heat loss should be carefully examined for any practical application. In situations with significant evaporation, the wall temperatures at large radius will be lower than the present predictions, although the evaporation rate will decline with increasing radius as a result of decreasing liquid surface velocity. For the present experiments, the evaporation effect is small.

Splattering has a strong effect on the wall temperature. It may cause decreases in the Nusselt number of up to 20% . The downstream flow is more seriously affected than the upstream flow. In most real systems, which are likely to be noisy and thus have splatter, this effect will reduce the efficiency of the jet in cooling the surface and increase the wall temperatures above the present predictions.

Nevertheless, the agreement between the theory and the present data is generally good, and confirms the trends predicted. Further experiments, in which the level of splatter is directly controlled, and a theoretical analysis of the role of splatter, are both needed. The possible effects of turbulence and of flow asymmetries also need further study.

The average Nusselt number for a constant heat flux is generally larger than for a constant wall temperature. Although the local Nusselt number for the plane jet is smaller than that for an axisymmetric jet in region 2 and part of region 3, the average Nusselt number for a plane jet is generally larger than that for an axisymmetric jet.

ACKNOWLEDGEMENTS

This work was supported by the A. P. Sloan Foundation and by the National Science Foundation under grant #CBT-8858288.

REFERENCES

Carper, H.J. and Deffenbaugh, D.M., 1978, "Heat transfer from a rotating disk with liquid jet impingement," *Proc. Sixth Intl. Heat Transfer Conf.*, Vol.4, Toronto, pp.113-118.

Carper, H.J., Saaveda, J.J., and Suwanprateep, T., 1986, "Liquid jet impingement cooling of a rotating disk," *J. Heat Transfer*, Vol.108, pp.541.

Chaudhury, Z.H., 1964, "Heat transfer in a radial jet," *J. Fluid Mech.*, Vol.20, pp.501-511.

Errico, M., 1986, "A study of the interaction of liquid jets with solid surfaces," Doctoral dissertation, University of California at San Diego, Chapter 3.

McMurray, D.C., Myers, P.S., and Uyehara, O.A., 1966, "Influence of impinging jet variables on local heat transfer coefficients along a flat surface with constant heat flux," *Proc. Third Intl. Heat Transfer Conf.*, Vol.2, Chicago, pp.292-299.

Metzger, D.E., Cammings, K.N., and Ruby, W.A., 1974, "Effects of Prandtl number on heat transfer characteristics of impinging liquid jets," *Proc. Fifth Intl. Heat Transfer Conf.*, Vol.2, Tokyo, pp.20-24.

Sharan, A., 1984,"Jet-disc boiling: burnout predictions and application to solar receivers," Master's thesis, University of Houston.

Watson, E.J., 1964, "The radial spread of a liquid over a horizontal plane," *J. Fluid Mech.*, Vol.20, pp.481-499.